GEOPHYSICS, VOL. 77, NO. 5 (SEPTEMBER-OCTOBER 2012); P. WC37–WC46, 16 FIGS., 2 TABLES.
10.1190/GEO2011-0478.1

Interpretation of 2D seismic profiles in complex geological terrains: Examples from the Flin Flon mining camp, Canada

D. J. White[1] and M. Malinowski[2]

ABSTRACT

A methodology was demonstrated for the 3D interpretation of networks of 2D seismic profiles in conjunction with other 3D geological constraints. The methodology employs 3D migration of 2D seismic data as a means of directly correlating reflections with out-of-plane geology, followed by ray-trace modeling of interpreted 3D geological surfaces. The proposed interpretation workflow was demonstrated with examples taken from 2D seismic profiles that were recently acquired for VMS ore exploration within the Flin Flon mining camp, Canada. In each example, the utility of the method was demonstrated and the resulting inferences were validated by comparison with a true 3D seismic survey acquired over a subset of the same area.

INTRODUCTION

Seismic reflection methods have found use in a variety of hardrock exploration applications during the last 20 years (e.g., Eaton et al., 2003, 2010). Although 3D surveys are essential to accurately defining exploration drill targets, 2D seismic profiles still have a useful role to play in mineral exploration because they provide an affordable means of making regional assessments, or of constructing sparse 3D geologic models from a network of seismic profiles. Also, 2D seismic surveys usually provide finer spatial sampling than 3D surveys due to the reduced number of shots and receivers required for 2D surveys to achieve a specific CDP bin width. However, interpretation of 2D images can be highly ambiguous when acquired across complex geologic environments. In such cases, auxillary information, in the form of surface-mapped structural attitudes, drillhole constraints and/or intersecting 2D profiles, is generally required to achieve geological interpretations that are geometrically accurate. Even then, interpretation is complicated by the fact that drillholes usually are deviated (3D) and seismic reflection lines often are crooked. Effective interpretation of 2D seismic data requires a methodology that facilitates correlation and interpretation of these combined data sets in 3D.

In this paper, we demonstrate a systematic approach to the 3D interpretation of multiple 2D seismic profiles as constrained by correlation with geology and logs from deviated drillholes. As such, this methodology is specifically suited for seismic-based exploration within regions where some drillhole information is available (e.g., mining camps). The methodology employs two well-known processes: 3D migration of 2D seismic data, and ray-trace modeling of geologic surfaces constructed during interpretation. The proposed interpretation workflow is demonstrated with examples taken from 2D seismic profiles that recently were acquired for VMS ore exploration within the Flin Flon mining camp (see Figure 1 for line locations). These profiles were processed using 2D crooked-line geometry with DMO and 2D poststack migration (Malinowski et al., 2008). In each example, the utility of the method is demonstrated and the resulting inferences are validated by comparison with a true 3D seismic survey acquired over a subset of the same area (White et al., 2012).

BACKGROUND

Two-dimensional seismic profiles acquired across 3D geology will comprise the superposition of reflections that generally derive from out-of-plane reflection points. In the simple case where the geology is 2D and the acquisition profile is oblique to the dip azimuth, the out-of-plane reflection raypaths lie within a common imaging plane (formed by the locus of reflection points and the acquisition line) that is inclined relative to the vertical. In the more general case of 3D geology, reflections may arrive from a spectrum of out-of-plane directions, and a common imaging plane only exists in some average sense, as illustrated in Figure 2. In this case, the resultant 2D stack image will represent the superposition of these various reflections onto a single arbitrarily chosen imaging plane

Manuscript received by the Editor 28 November 2011; revised manuscript received 7 March 2012; published online 6 September 2012.
[1]Geological Survey of Canada, Ottawa, Ontario, Canada. E-mail: don.white@nrcan.gc.ca.
[2]Polish Academy of Sciences, Institute of Geophysics, Warsaw, Poland. E-mail: michalm@igf.edu.pl.

(e.g., Figure 2b), usually chosen as the vertical plane beneath the acquisition line. Two-dimensional migration is usually applied to reposition these reflections within the chosen imaging plane, a process which will be inaccurate to varying degrees, depending on how oblique the acquisition line is to the local geological dip azimuth. Crooked 2D acquisition lines accentuate the complications associated with this process (e.g., Wu, 1996).

Other geometric constraints must be applied to reduce the ambiguity in the interpretation of 2D images. In the case of crooked 2D acquisition lines, identification of out-of-plane reflections can be partially assessed directly from the data by application of various prestack processing methods, including cross-dip analysis (e.g., Wu et al., 1995; O'Dowd et al., 2004), swath-3D processing (Malehmir et al., 2009), azimuthal binning (Kashubin and Juhlin, 2010; Lundberg and Juhlin, 2011), or 3D prestack migration (Nedimovic and West, 2003). However, the effectiveness of such approaches will vary case-by-case, because they depend on the crooked nature of the acquisition line. Alternatively, 3D poststack migration can be applied directly to the 2D DMO-stacked data. This process, though recognized as being valid (e.g., Sheriff and Geldart, 1984, p. 326), is not commonly applied to 2D data for several reasons: First, the lack of aperture in the out-of-plane direction yields highly smeared images for crossline sections, limiting their usefulness; second, although inline sections from the 3D volume provide well-resolved images, there is no basis for preferentially choosing any of the inline sections from the 3D volume over that which corresponds to the simple 2D migration. In light of these first two reasons, the computational expense of applying 3D migration over 2D migration is not justified. However, these ambiguities can be partly addressed using auxiliary data, such as drillhole information. The 3D migration process distributes energy from a specific reflection observed on the 2D stacked section over a surface in 3D that is consistent with the observed two-way reflection traveltimes. This 3D surface does not correspond to a 3D reflector (i.e., geologic horizon), but its intersection with the (unknown) imaging plane defines a trace along the reflector in 3D. Thus, the spatial coincidence of this 3D surface with geologic contacts from drillholes can be assessed directly as a means of evaluating the contact as the source of the observed reflections. Commonly available 3D seismic visualization and interpretation tools can be used for this purpose.

This 3D migration process is shown schematically in Figure 3 for the simple case of an oblique acquisition line that crosses a dipping reflection. The normal-incidence raypaths and their associated imaging points on the reflector are shown in Figure 3a. These raypaths define the imaging plane. Also shown are the corresponding positions of these points on the vertical plane beneath the acquisition line. As shown schematically in Figure 3b, 3D migration spreads the energy from each of the points on the unmigrated vertical section over a spherical surface whose center is located at the acquisition recording point and whose radius is the distance associated with the two-way reflection traveltime. The envelope of the spherical surfaces defines a 3D surface whose intersection with the vertical acquisition plane corresponds to the conventional 2D migration (Figure 3c). As expected, the 2D migrated reflection on the vertical section has a shallower dip than the reflector where it is intersected by the vertical plane. The intersection of the 3D migration surface with the imaging plane (defined by the raypaths in Figure 3a) defines the trace of the actual imaging points on the reflector in 3D. The 3D migration surface is tangential to the reflector along this trace.

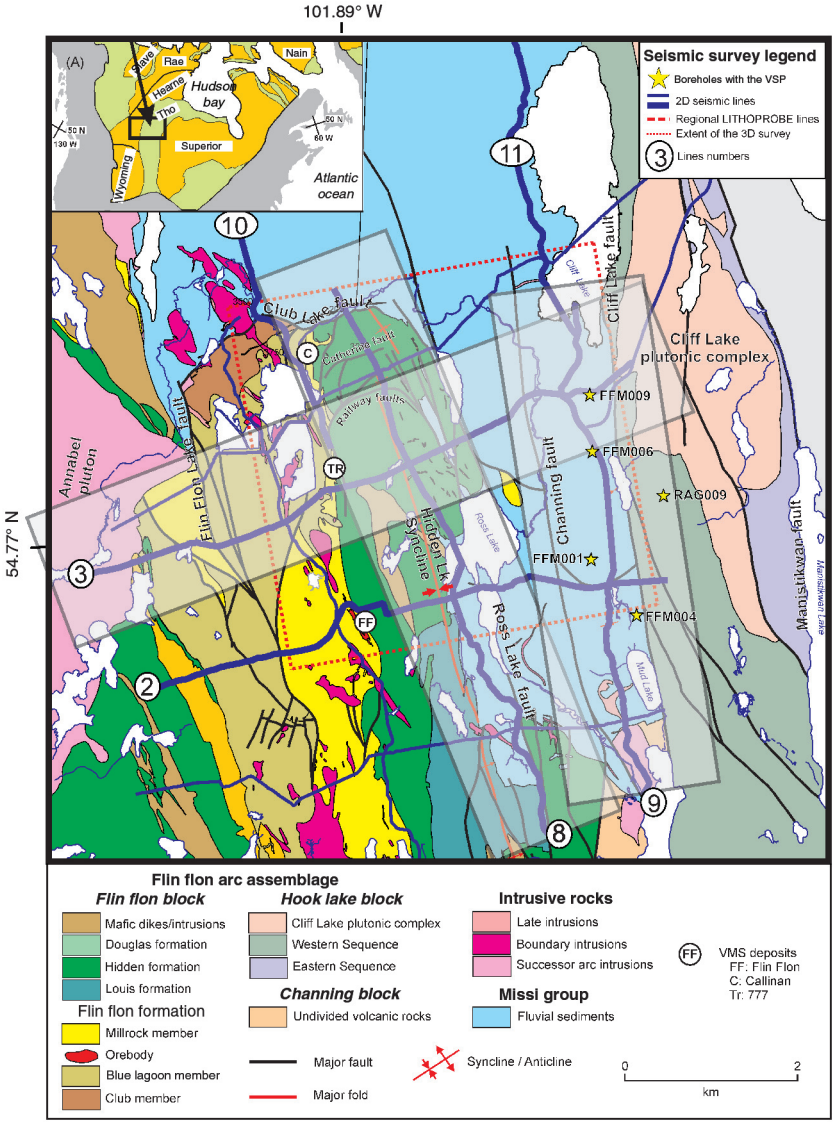

Figure 1. Geologic map of the Flin Flon mining camp showing the locations of the 2D seismic profiles. Inset (upper left) shows the location within the major Precambrian provinces of North America (THO = Trans-Hudson Orogen). The gray shaded rectangles show the outlines of the volumes used for 3D migration of the 2D data.

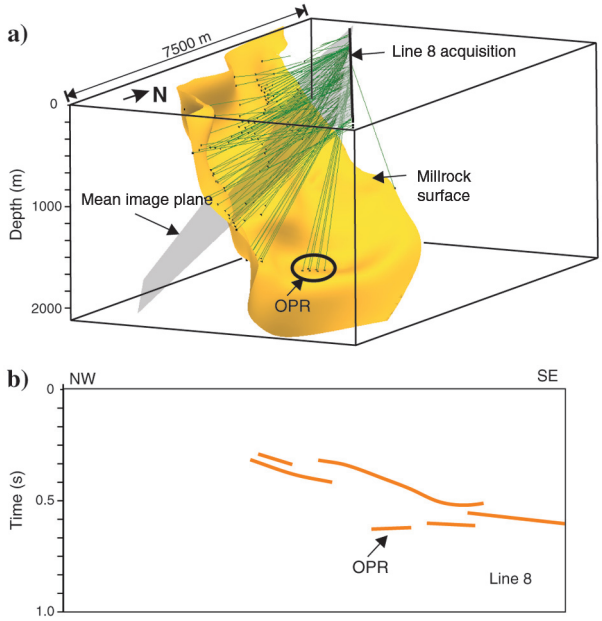

Figure 2. (a) A representative 3D geologic surface from the Flin Flon mining camp (Millrock member; see Figure 1) is shown in relation to an oblique acquisition line (Line eight; see Figure 1). As can be seen, the raypaths (green lines) illuminating the Millrock surface for seismic acquisition along Line eight generally arrive from out-of-plane. The mean imaging plane depicted is inclined relative to the vertical. (b) Schematic of the unmigrated reflections (in two-way traveltime) corresponding to the raypaths in (a), is shown projected onto a vertical section as is the common practise. OPR = out-of-plane reflection.

There are several distinct advantages in applying 3D migration to 2D data: (1) It allows direct correlation of the seismic images with external geologic constraints, without an intervening interpretation or modeling step; (2) more consistent ties are achievable between intersecting 2D seismic lines; (3) migration of crooked 2D profiles is accomplished in a more rigorous manner than simple projection onto a plane prior to migration. Geologic contacts can be extrapolated away from the drillholes using the geometrical constraints provided by the seismic horizon. A disadvantage of the method is that correlation of seismic reflections can only be made with geologic contacts that lie up-dip in the out-of-plane direction relative to the 2D seismic line.

METHOD

The utility of 3D-migration of 2D crooked line data is demonstrated in interpretation of seismic data from the 2007 Flin Flon seismic program. The 2D data from this program were processed to DMO stack using a conventional time-processing sequence (see Tables 1 and 2 for acquisition and processing details). CDP binning was implemented along crooked slalom lines (e.g., Figure 4) with a 2.5 m inline bin width. Three-dimensional migration of the 2D data was accomplished using the following steps: A 3D volume was constructed with 5×5 m bins containing zero amplitude traces. A rectangular 3D volume extending 900 m to either side of the 2D seismic profile (see Figure 4) was designed to accommodate crossline migration of reflections for moderate crossline dips to depths of up to ~1500 m. The original 2D DMO stack was decimated from the original 2.5 m bins to 5 m bins to match the bin dimensions of the 3D seismic volume. The resultant traces were used to populate the 3D volume at CDP locations corresponding to

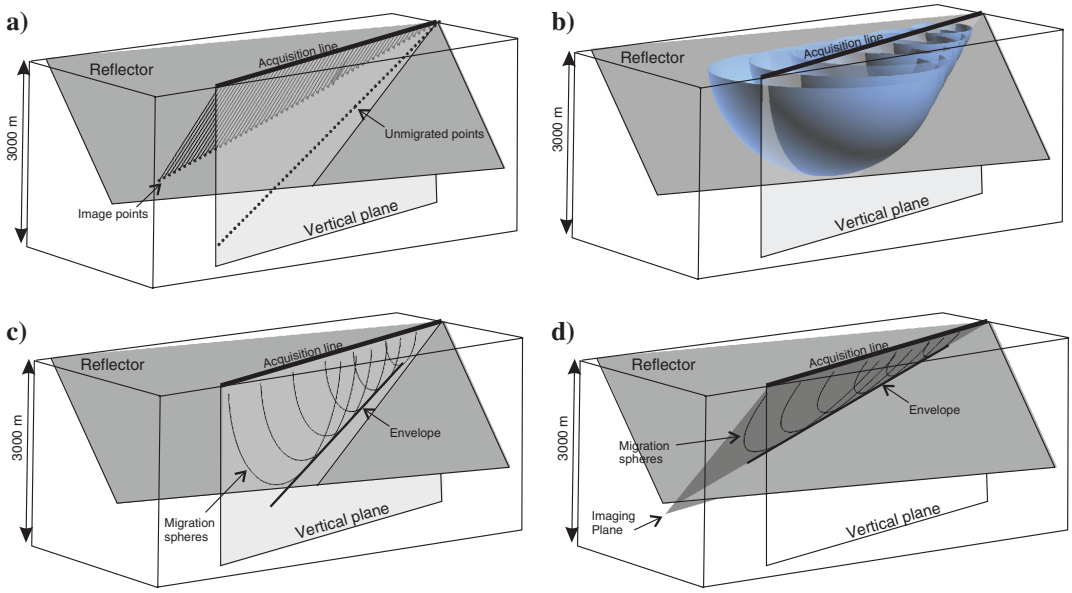

Figure 3. Schematic of the 3D migration of 2D seismic data for a constant velocity medium. (a) Oblique acquisition line oriented at 30° to the strike of a reflector that dips at 45°. Normal incidence raypaths are shown along with the resultant location of the unmigrated reflections on the vertical plane beneath the acquisition line. (b) Spherical surfaces depicting the geometry of 3D constant velocity migration. Energy from each of the unmigrated reflection points in (a) is spread across the corresponding spherical surface. (c) The envelope of the spherical surfaces where they cut the vertical plane corresponds to the conventional 2D migration of the data. (d) The envelope of the spherical surfaces where they cut the imaging plane corresponds to the trace of actual imaging points along the reflector in 3D.

the 2D binning line (either a straight line or a sinuous slalom line, as shown in Figure 4). This construction process results in a sparsely occupied 3D volume having nonzero amplitude traces only within those 3D bins which are spatially coincident with the corresponding 2D CMP bin locations. For the 3D volume geometry chosen, typically $<0.3\%$ of the volume has nonzero values prior to migration. Constant velocity 3D phase-shift migration was subsequently applied to this volume.

RESULTS

The first example illustrates the process for a 2D profile (Line nine, Figure 5) that images a thick succession of metasedimentary rocks (the Missi Group; Figure 1) that is interleaved with thrust panels of mafic volcanic rocks (e.g., V1A and V1B, in Figure 5a). Locating the volcanic rocks as either basement or thrust panels beneath the Missi Group is a key exploration objective because the volcanic rocks could be an extension of the geology hosting the known Flin Flon ore deposits. Contacts between the mafic volcanic rocks and the Missi sandstones are know to be highly reflective (e.g., White et al., 2008). Originally the data were processed using the straight binning line shown in Figure 4. Figure 5a shows the original 2D migration of Line nine. Trace mixing and decimation into 5-m bins were applied to allow direct comparison with the corresponding section extracted from the 3D migration (Figure 5b). The 3D migration was achieved using the process described in the preceding section. There is little difference in the reflection image obtained from the 2D migration and the 3D migration observed along a coincident vertical section. Constant velocity migrations were conducted in this case and in all of the examples that follow. Individual migration velocities ranged from 5000 to 5400 m/s, unless otherwise stated, and were generally based on the comparison of migrations of the true 3D data with the geometry of known geologic horizons.

Table 1. Seismic acquisition parameters.

Source types	Vibroseis and dynamite
Shot interval	20 m
Vibe configuration	2×24000 kg IVI Y-2400 (Mark-IV) Vibes "Nose-to-tail"
Vibe sweeps	Three to five 15 s sweeps, 30–160 Hz nonlinear with 3 dB per octave boost
Dynamite shots	500 gm in 5 m drillholes
Receiver types	Single I/O Vectorseis SVSM 3C sensor at each receiver station
Receiver interval	5 m
Receiver spread	600-station (1800 channel) symmetric split spread

Table 2. Data processing flow.

Geometry setup (crooked line)
CDP inline bin width: 2.5 m
Refraction statics
True amplitude recovery (either 6 db/s or t^2)
Surface consistent amplitude scaling
Phase rotation for vibroseis data (−90°)
Top mutes (~30 ms postfirst breaks except on inner traces)
Surface consistent predictive deconvolution
Automatic gain control (200 ms)
Spectral whitening (35/40–130/140 Hz; eight panels)
Normal moveout correction (V_{rms} = 6000 m/s)
Residual statics (Power maximization; max 10 ms shift)
Partial prestack migration (time domain DMO) in shot domain
Common-depth-point stack
Phase-shift migration (5000–6000 m/s)
F-X deconvolution
Time-variant scaling
Time-to-depth conversion using 6000 m/s

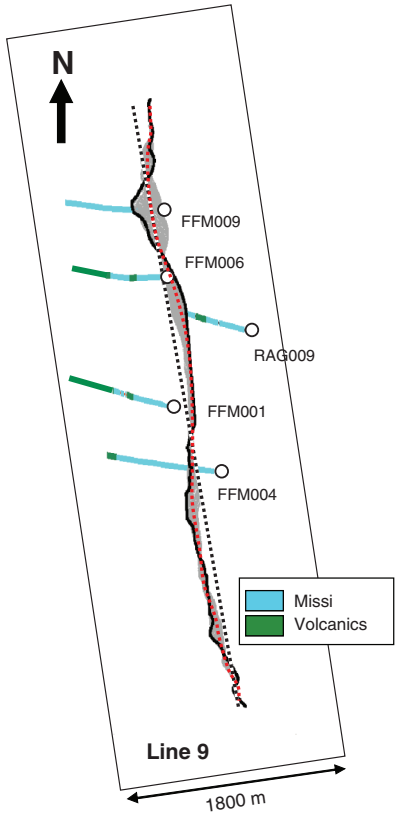

Figure 4. Geometry of Line nine from the Flin Flon survey (see Figure 1 for location) showing the acquisition line (black line), the smooth CMP positions (dashed red line), the scatter of the reflection midpoints (gray cloud), and the line of the 2D imaging plane (straight dashed line). The rectangle encompassing the survey line denotes the extent of the 3D volume constructed for migration of the 2D data. Also shown are the plan view projections of the deviated drillholes along the line. The legend for drillhole geology applies to all subsequent figures.

The utility of the 3D migrated data becomes apparent when we try to correlate the seismic data with the available drillhole geology. As can be seen in Figure 4, the drillholes are deviated and generally lie 100 to 600 meters west of the 2D profile. Qualitative comparison of the depth of known impedance contrasts between the metasedimentary rocks and the mafic volcanic rocks suggests that contacts between these units are likely responsible for the prominent reflections observed along this profile. The 3D migrated data of Line nine allow direct testing of this hypothesis. As can be seen in Figure 6, a prominent bright reflection (labeled V1A) as imaged on an inline section 350 m west of Line nine, is spatially coincident with a mafic volcanic horizon intersected in drillhole FFM006. Similarly, reflection V1B (Figure 7) as imaged on an inline section 565 m west of Line nine, is coincident with a deeper mafic volcanic horizon intersected in drillhole FFM001. Strictly speaking, it only can be said that the locations of these contacts as observed in the drillholes is consistent with the observed seismic data. If there are sufficient geologic constraints to determine the local orientation of the geological contact (e.g., dip information from individual drillholes or multiple drillhole intersections) ray-tracing can be done to further test the correlation as demonstrated in the next example. However, in the present case, comparison with the true 3D seismic data (Figure 8) confirms the interpretation.

The second example is from an orthogonal line (Line three) that crosses a shallow ore zone. The Callinan ore deposit (see White et al., 2012 for further description) comprises several large lenses that are 600 to 1000 m long and less than 200 m wide, and vary in thickness ranging from less than 10 m up to 30 m. They dip moderately to the east or east-southeast. Line three is oriented at $\sim 20-30^{\circ}$ relative to the dip direction; thus, out-of-plane reflections/diffractions from the ore zone are expected. Figure 9a and 9b shows the Line three stack and 2D migration, respectively, with the intersection of the Callinan ore zone superposed. A prominent diffraction is observed in Figure 9a, with the strongest amplitudes occurring in the down-dip direction. The migrated stack (Figure 9b) shows a reasonably good correlation of a short, prominent, east-dipping reflection with the known ore zones. However, closer inspection reveals that the migrated reflection lies somewhat down-dip from the ore zones. Figure 9c shows an inline section from the 3D migration of Line three. This section is located ~135 m to the north of the 2D profile. The prominent reflection on this section provides a better spatial correlation with the ore zone, indicating that the image corresponds to a portion of the ore zone located north of the 2D imaging plane. This correlation is further supported by ray-tracing results, as shown in Figure 10, which illustrate that ore zone reflections originating as far out-of-plane as 300 m provide a good match to the observed diffraction traveltimes. Furthermore, the zone having the highest density of reflected arrivals (a proxy for higher amplitudes) in Figure 10 corresponds to the strongest amplitudes observed along the hyperbolic diffraction trajectory on the seismic section. This

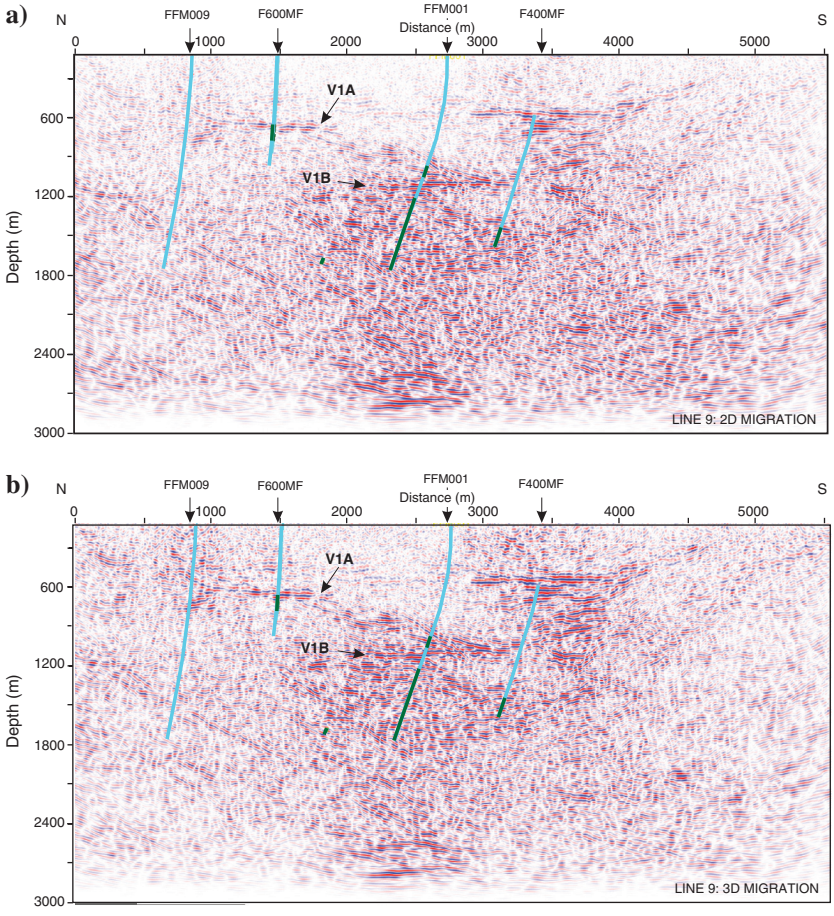

Figure 5. Comparison of 2D and 3D migrations for Line nine. Prior to either migration, the DMO stack was decimated to 5 m trace spacing (from 2.5 m) and a three-trace mix was applied. (a) Two-dimensional Stolt migration for frequency range of 10-130 Hz. A straight-line fitted to the CDP slalom line (see Figure 4) was used as the imaging plane. (b) Stolt 3D migration of Line nine with the same frequency band as in (a). A slice through the volume is shown, which corresponds to the imaging plane used in (a). For the 3D migration, the Line nine DMO stack data were placed into a 3D cube constituted of zero-amplitude traces. The data traces were inserted at positions corresponding to the smooth CMP line from Figure 3. V1A and V1B denote reflections associated with volcanic horizons described in Figure 4. The generalized geology from deviated drillholes also is shown. A constant velocity of 6000 m/s was used for the time-to-depth conversion of the seismic data.

out-of-plane correlation is confirmed by a comparison with the true 3D seismic volume (Figure 11).

Example three is from a profile (Line eight) that is oriented subparallel to the plunge-line of the Callinan and 777 ore deposits. Figure 12 shows the geometry of the acquisition line relative to the orebodies which lay several hundred meters to the west of the profile. The ore bodies dip moderately to the east or east-southeast (i.e., toward the seismic profile). Clearly, the only manner of imaging the orebodies along Line eight would be through the observation of out-of-plane reflections. To test this hypothesis, inline sections through the 3D migration of Line eight are shown in Figures 13 and 14, along with the corresponding intersections with the ore zones (known from extensive drilling). As can be seen, there is a very good correlation of the ore zone geometries with the reflectivity as observed on the 3D migrated sections that are located 200–350 m to the west of the 2D seismic profile. This interpretation generally is confirmed by comparison of the DMO stack with reflection traveltimes for the ore zones (Figure 15) that were calculated by normal-incidence, constant-velocity (6000 m/s) ray-tracing.

Identification of reflections from a common reflector as observed on two crossing seismic lines provides the means of determining the true local orientation of the reflector. An example of this is shown in Figure 16a where reflections V1B and V2 are observed at the intersection of Lines two and nine. In general, reflections originating from a common reflector should occur at the same two-way traveltime at the intersection of the stack sections, although in practice this is not always the case for crooked acquisition/processing lines. In that the stack section represents an approximate zero-offset section, the coincidence of reflections should occur even for out-of-plane reflections. The apparent dip of the reflection at the tie point on the stack section provides input information to calculate the true attitude of the reflection. Direct migration of the 2D lines will give reflection dips that are inaccurate if an out-of-the-plane dip component is present, and the reflections will no longer tie at the intersection because they will be improperly migrated (i.e., undermigrated)

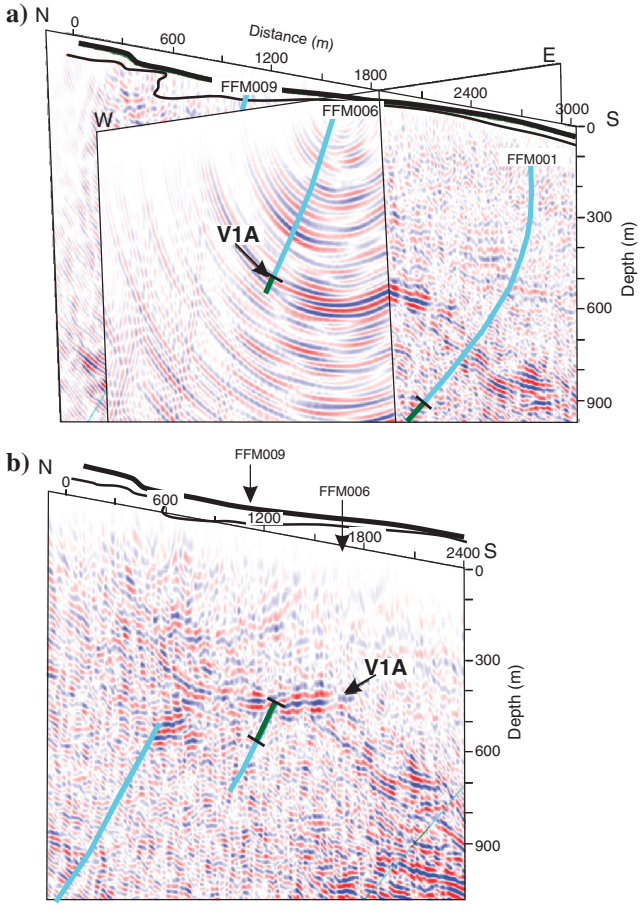

Figure 6. Line nine 3D migration. (a) Fence-diagram showing the reflection event V1A on the original 2D section and how it migrates orthogonal to the acquisition line when 3D migration is applied. (b) Inline section from the Line nine 3D migration. This section is located 350 m to the west of Line nine, and shows the correlation of reflection V1A with the basalt contact in drillhole FFM006. A constant velocity of 6000 m/s was used for the time-to-depth conversion of the seismic data.

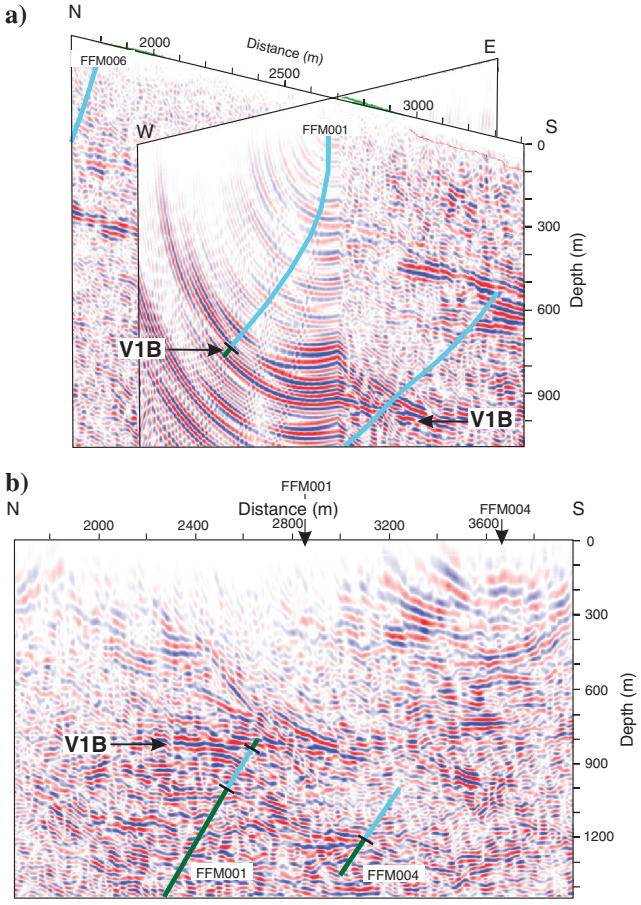

Figure 7. Line nine 3D migration. (a) Fence-diagram showing the reflection event V1B on the original 2D section and how it migrates orthogonal to the acquisition line when 3D migration is applied. (b) Inline section from the Line nine 3D migration. This section is located 565 m to the west of Line nine, and shows the correlation of reflection V1B with the basalt contact in drillhole FFM001. A constant velocity of 6000 m/s was used for the time-to-depth conversion of the seismic data.

in the plane of the sections. This can be seen in Figure 16b. Three-dimensional migration of the intersecting 2D profiles can help to resolve this ambiguity. It allows comparison of the reflection ties at their true spatial position and at the correctly migrated orientation. Inline sections from the 3D volumes for each profile can be inspected in the vicinity of the intersection of the profiles to find where the migrated reflections intersect. This is demonstrated in Figure 16c where a Line nine inline section located ~150 m west of the Line nine profile shows a good tie for reflections V1B and V2

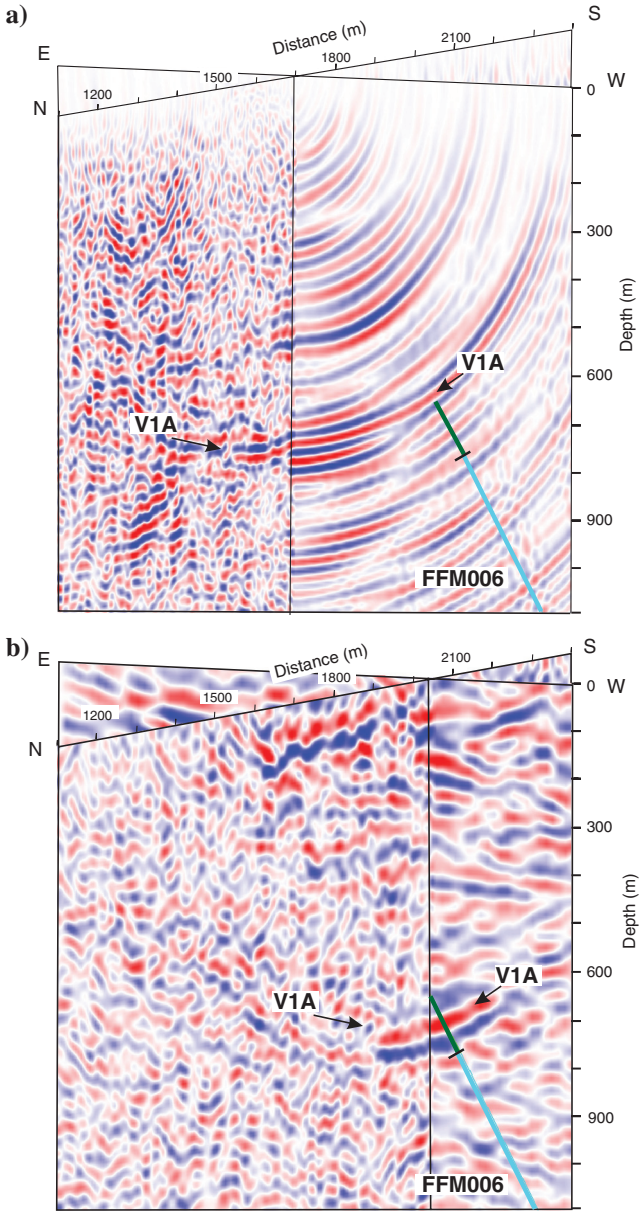

Figure 8. Comparison of Line nine 2D data with true 3D data. (a) Inline and crossline sections from the 3D migration of Line nine (same as Figure 6). (b) Fence diagram from the true 3D cube (see White et al., 2012) confirming the 2D interpretation of this reflection along Line nine. A constant velocity of 6000 m/s was used for the time-to-depth conversion of the seismic data.

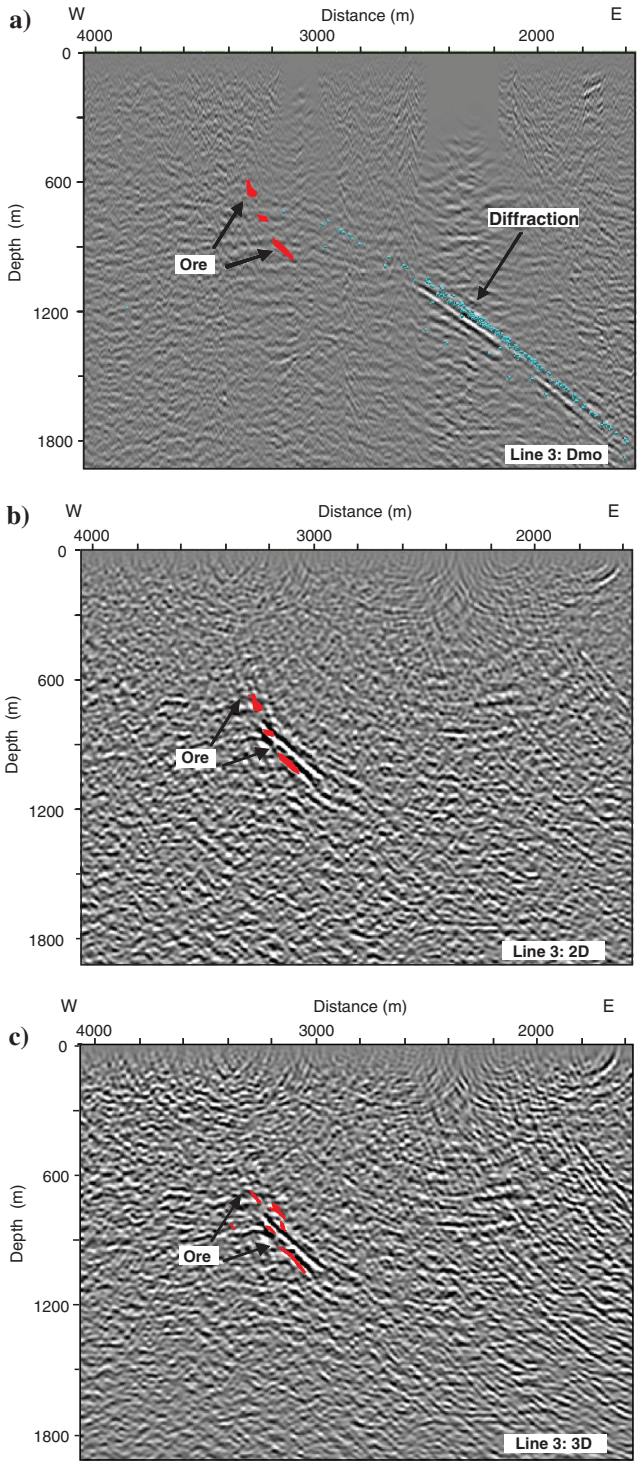

Figure 9. (a) Line three DMO stack showing diffraction response from the Callinan ore lenses (superposed in all panels). Note that the positions of the reflection traveltimes from ray tracing (blue symbols) have been shifted up by 50 m so that the corresponding reflections can be clearly seen. (b) Line three 2D migration of the DMO stack. (c) Line three vertical section through the 3D migration of the 2D DMO stack. This vertical section is located 135 m to the north of the 2D imaging plane. Migrations and time-to-depth conversions used a velocity of 6000 m/s. A constant velocity of 6000 m/s was used for the time-to-depth conversion of the seismic data.

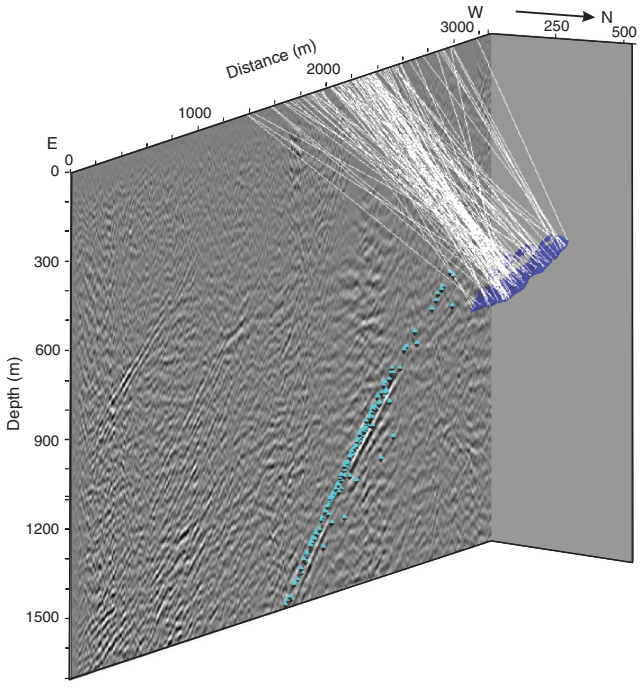

Figure 10. Perspective view of the Line three DMO image, with raypaths (white lines) for normal-incidence reflections from the Callinan ore lenses (blue body). The ore lenses plunge into the seismic section (from right to left). The reflections from the ore zone observed along Line three originate from as far as 300 m in the out-of-plane up-plunge direction. The traveltimes as determined by normal incidence ray tracing also are shown (blue points) on the seismic image. A constant velocity of 6000 m/s was used for the time-to-depth conversion of the seismic data.

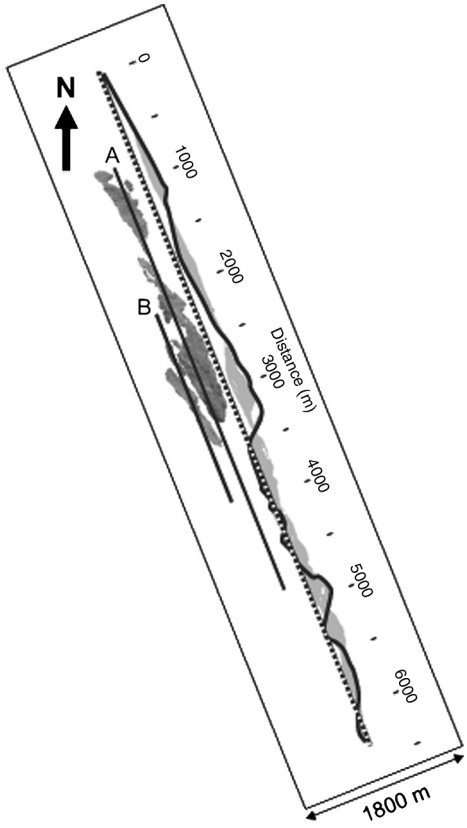

Figure 12. Line eight survey line (solid black line), CDP scatter points (light gray), and CDP binning line (dashed line) used for 2D processing. The orebodies (dark gray bodies) dip to the east and plunge toward the SSE. The locations of the sections shown in Figures 13 and 14 are indicated by the transects labelled A and B, respectively.

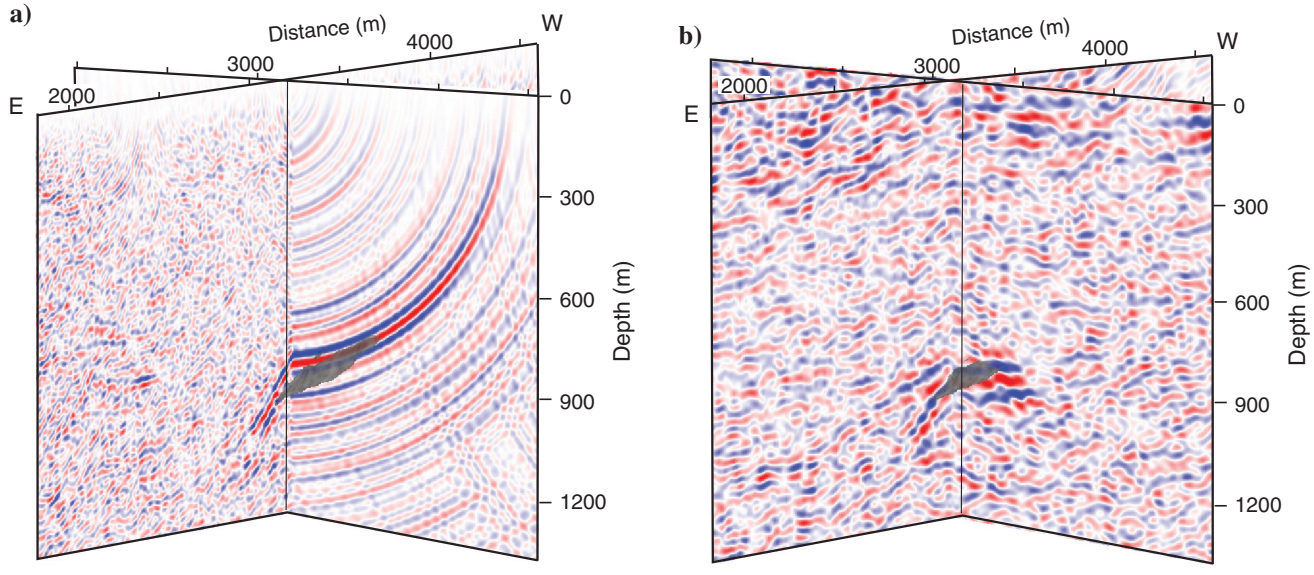

Figure 11. (a) Inline and crossline sections from the 3D migration of Line three showing the correlation with the Callinan ore lens (gray body) in the up-plunge direction. (b) Similar orthogonal sections from the true 3D migrated volume. A constant velocity of 6000 m/s was used for the time-to-depth conversion of the seismic data.

at the intersection with an inline section for Line two. A further requisite for these ties to be authentic is that the orientation is consistent as observed on both 3D-migrated sections. Comparison of the apparent reflection dip as observed along Line two (Figure 16c) with that on a Line nine crossline (Figure 16d) shows this to be the case. Thus, the use of 3D migration allows accurate determination of the true local position and orientation of the reflector as observed on intersecting profiles.

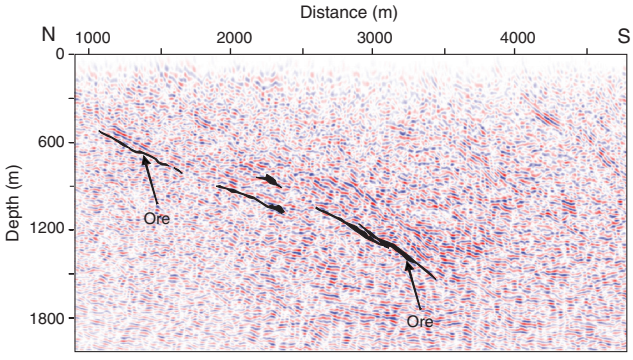

Figure 13. Vertical section through the 3D-migration of Line eight, taken approximately 200 m west of the acquisition line. Note that the positions of the ore intersections have been shifted down by 60 m so that the corresponding reflections can be clearly seen. There is a good correspondence between the ore zone geometries and the seismic data. A constant velocity of 6000 m/s was used for the time-to-depth conversion of the seismic data.

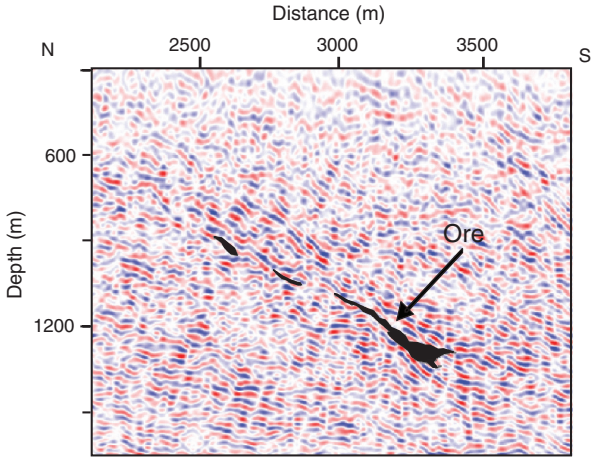

Figure 14. Vertical section through the 3D-migration of Line eight, taken approximately 350 m west of the acquisition line. There is a good correspondence between the deeper 777 ore zone geometry and the seismic data. A constant velocity of 6000 m/s was used for the time-to-depth conversion of the seismic data.

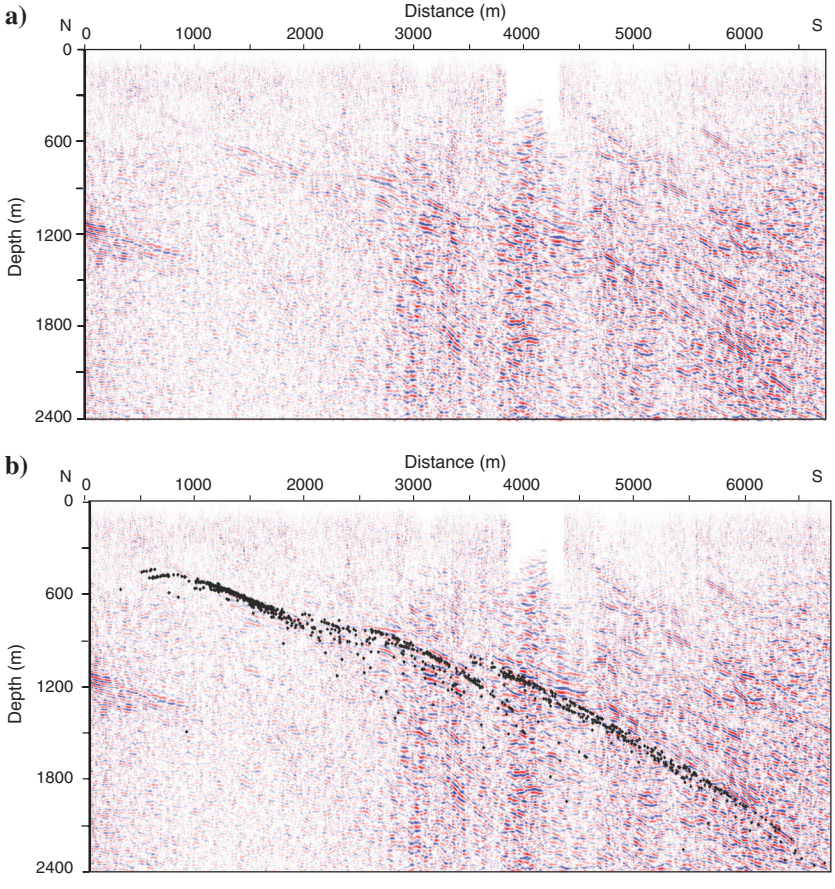

Figure 15. (a) DMO stack for part of Line eight. (b) Same as (a), but with traveltimes superposed that were determined by normal-incidence ray tracing from the orebodies shown in Figure 12. A constant velocity of 6000 m/s was used for the time-to-depth conversion of the seismic data.

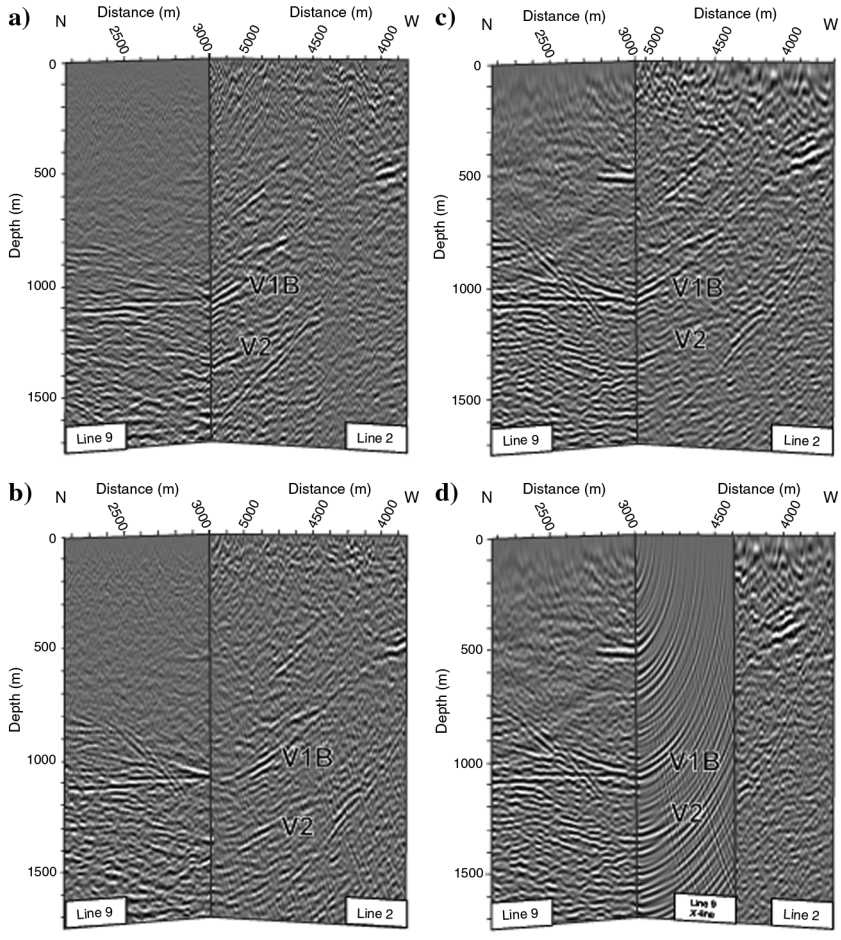

Figure 16. Reflection ties at intersection of profiles two and nine. (a) Unmigrated DMO stacks, (b) 2D migrated DMO stacks, (c) inline sections from 3D migrations of Lines two and nine, and (d) inline and crossline section from 3D migration of Line nine. In (c) and (d), the Line nine section shown is located ~150 m west of the survey line to account for the easterly dips. Note the improved ties for the two shallow reflections (V1B and V2) in (c) as compared to (b). A constant velocity of 6000 m/s was used for the time-to-depth conversion of the seismic data.

CONCLUSIONS

Three-dimensional poststack migration of 2D seismic data, combined with subsequent ray-trace modeling of constructed geologic surfaces, can provide an effective means of interpreting multiple 2D seismic profiles with external 3D geological constraints. As such, this methodology is applicable for seismic-based mineral exploration within regions where some drillhole information is available. The use of drillhole constraints or other auxiliary structural information reduces the ambiguity inherent in 2D seismic reflection images acquired across complex geologic terrains, and increases the utility of applying 3D migration to 2D data. Advantages of applying 3D migration to 2D data, as demonstrated by examples presented here, include (1) a capability for linking seismic reflections to known geologic contacts through direct imaging (as opposed to modeling alone) (2) improved correlation of seismic reflectors at the intersections of profiles, and (3) proper migration of crooked 2D profiles. Three-dimensional geologic interpretations of 2D data in the examples presented were verified using true 3D seismic data available for part of the study area. This methodology has been used in the 3D interpretation of a network of seismic profiles from the Flin Flon mining camp.

ACKNOWLEDGMENTS

Two-dimensional seismic data were acquired as part of the Geological Survey of Canada's Targeted Geoscience Initiative-3 Project. Hudson Bay Mining and Smelting Co. funded the acquisition and processing of the 3D seismic data, partially funded 2D seismic data acquisition, and provided extensive drillhole information to the project. Brett Pearson and Jason Levers (HBMS) provided details of the ore deposits. The seismic data were acquired by Kinetex Inc. Ernst Schetselaar provided digital geologic data, and Barbara Dietiker provided drafting support. MM was supported by the HOMING scholarship from the Foundation for Polish Science. This is Geological Survey of Canada contribution number 20110302. The authors acknowledge informative critical reviews by Kris Vasudevan, Chris Juhlin, Doug Schmitt, and Gilles Bellefleur.

REFERENCES

Eaton, D. W., E. Adam, B. Milkereit, M. Salisbury, B. Roberts, D. White, and J. Wright, 2010, Enhancing base-metal exploration with seismic imaging, in lithoprobe: Parameters, processes and the evolution of a continent: Canadian Journal of Earth Sciences special issue, **47**, 741–760, doi: 10.1139/E09-047.

Eaton, D. W., B. Milkereit, and M. H. Salisbury, eds., 2003, Hardrock seismic exploration: Geophysical Development Series, no. 10, SEG.

Kashubin, A. S., and C. Juhlin, 2010, Mapping of crustal scale tectonic boundaries in the Ossa-Morena zone using reprocessed IBERSEIS reflection seismic data: Tectonophysics, **489**, 139–158, doi: 10.1016/j.tecto.2010.04.010.

Lundberg, E., and C. Juhlin, 2011, High-resolution reflection seismic imaging of the Ullared deformation zone, southern Sweden: Precambrian Research, **190**, 25–34, doi: 10.1016/j.precamres.2011.07.012.

Malehmir, A., C. Schmelzbach, E. Bongajum, G. Bellefleur, C. Juhlin, and A. Tryggvason, 2009, 3D constraints on a possible deep >2.5 km massive sulphide mineralization from 2D crooked-line seismic reflection data in the Kristineberg mining area, northern Sweden: Tectonophysics, **479**, 223–240, doi: 10.1016/j.tecto.2009.08.013.

Malinowski, M., D. J. White, C. J. Mwenifumbo, M. Salisbury, G. Bellefleur, D. Schmitt, B. Dietiker, E. Schetselaar, and A. Duxbury, 2008, Seismic exploration for VMS deposits within the paleoproterozoic Flin Flon belt, Trans-Hudson Orogen, Canada: 70th Annual International Conference and Exhibition, EAGE, Extended Abstracts, 216.

Nedimovic, M. R., and G. F. West, 2003, Crooked-line 2D seismic reflection imaging in crystalline terrains: Part 2, migration: Geophysics, **68**, 286–296, doi: 10.1190/1.1543214.

O'Dowd, C. R., D. Eaton, D. Forsyth, and H. W. Asmis, 2004, Structural fabric of the central metasidementary belt of southern Ontario, Canada, from deep seismic profiling: Tectonophysics, **388**, 145–159, doi: 10.1016/j.tecto.2004.07.041.

Sheriff, R. E., and L. P. Geldart, 1984, Exploration seismology, 2nd ed.: Cambridge University Press.

White, D., M. Malinowski, P. Cary, and D. Secord, 2008, 2D/3D multi-component seismic imaging in the Flin Flon mining camp, Canada: 78th Annual International Meeting, SEG, Expanded Abstracts, 3609–3612.

White, D. J., D. Secord, and M. Malinowski, 2012, 3D seismic imaging within the Flin Flon VMS mining camp: Geophysics, this issue.

Wu, J., 1996, Potential pitfalls of crooked-line seismic reflection surveys: Geophysics, **61**, 277–281, doi: 10.1190/1.1443949.

Wu, J., B. Milkereit, and D. E. Boerner, 1995, Seismic imaging of the enigmatic Sudbury structure: Journal of Geophysical Research, **100**, 4117–4130, doi: 10.1029/94JB02647.